REACTION KINETIC PARAMETERS FOR ION TRANSPORT FROM STEADY-STATE CURRENT–VOLTAGE CURVES

D. GRADMANN,* H.-G. KLIEBER,* AND U.-P. HANSEN‡
*Pflanzenphysiologisches Institut und Botanischer Garten der Universität, Untere Karspüle 2, D-3400 Göttingen, Federal Republic of Germany; and ‡Institut für Angewandte Physik, D-2300 Kiel, Federal Republic of Germany

ABSTRACT This study demonstrates possible ways to estimate the rate constants of reaction kinetic models for ion transport from steady-state current–voltage data as measured at various substrate concentrations. This issue is treated theoretically by algebraic reduction and extension of a reaction kinetic four-state model for uniport. Furthermore, an example for application is given; current–voltage data from an open K^+ selective channel (Schroeder, J. I., R. Hedrich, and J. M. Fernandez, 1984, *Nature (Lond.)*, 312:361–362) supplemented by some new data have been evaluated. The analysis yields absolute numerical estimates of the 14 rate constants of a six-state model, which is discussed in a wider context.

INTRODUCTION

For ion transport through lipid membranes, Läuger (1980) has demonstrated the theoretical principles of a unified reaction kinetic model, irrespective of the physical mechanism or the physiological function of the particular transporters, e.g., carriers, channels, pumps, uni-, sym-, and antiporters. The general model is cyclic and describes not only the movement of charges across a series of energy barriers in the transporter but also the reorientation of the uncharged binding site(s), which may become rate limiting. One application of this theory is to calculate the steady-state current–voltage relationships of transporters for various experimental conditions, providing their architecture and rate constants are known. For practical use, however, it is more important and usually more difficult to solve the inverse problem, i.e., to obtain the model parameters from experimental data, e.g., from current–voltage curves. Steady-state data have been considered inappropriate for the solution of the inverse problem (Eigen, 1968; Läuger, 1973). The analysis of temporal transients has preferentially been applied in the past.

However, nonlinear steady-state current–voltage curves do contain the necessary information to determine some or even all rate constants of an assumed reaction scheme, depending on the particular conditions. In the first part of this paper we present a theoretical examination of this solution of the inverse problem using the concept of gross rate constants and reserve factors, which has been introduced by Hansen et al. (1981). In the second part we demonstrate an application by analyzing previously published data that are supplemented by some new data from the same series of patch-clamp experiments on a selective potassium channel in the plasmalemma of guard cell protoplasts from *Vicia faba* (Schroeder et al., 1984).

The analysis focuses on a four-state model for uniport with a symmetric Eyring barrier in one of the four reversible reaction steps. To account for the effects of a competing substrate, this model is extended to a six-state model. It is demonstrated that this model provides an adequate description of the data and that all parameters of the extended model can be extracted from the experimental information.

THEORY

Definitions and Nomenclature

We mainly consider here a uniporter, X, for a transportee, S, which carries the charge ze across a membrane (z being the charge number and e the elementary charge). The quantity of X enters the description of membrane currents only as a scaling factor, either as a density (moles of X per unit area of membrane, where macroscopic membrane currents are concerned) or as the actual number of molecules. The transporter operates in a reaction cycle through (at least) four distinct states (cf. Fig. 1 *A*): (*a*) occupied binding site facing cytoplasmic side (inside), (*b*) occupied binding site facing extraplasmic side (outside), (*c*) empty binding site facing outside, and (*d*) empty binding site facing inside.

The reversible transitions from one state to an adjacent one are described by pairs of rate constants. A cycle of four states is described by eight rate constants. Transporters for more than one transportee (cotransporters) or with additional reactants (e.g., ATP, inhibitors, etc.) require more states and rate constants for an adequate description of every essential reaction step involved (cf. Figs. 3 and 6).

Since models with various numbers of states (mainly four, and reduced models with three and two states) are to

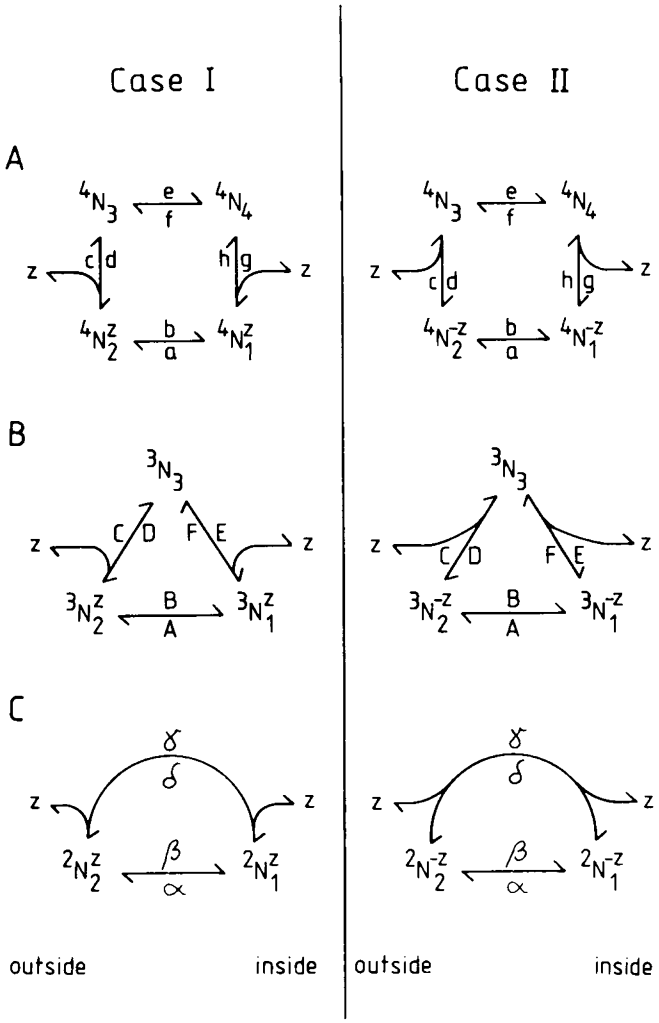

FIGURE 1 Nomenclature used for reaction-kinetic description of a cyclic reaction scheme for uniport of ions with the charge ze across a lipid membrane. (*A*) Minimum model with four states (probabilities $^4N_1$ to $^4N_4$) and eight rate constants (a to h; a and b are voltage-sensitive) for explicit description of individual reactions. (*B*) Reduced model with three states (probabilities $^3N_1$ to $^3N_3$) and six rate constants (A to F; A and B are voltage-sensitive). (*C*) Final reduction to model with two states (probabilities $^2N_1$ and $^2B_2$) and four rate constants (α to δ; α and β are voltage-sensitive). Case I, unoccupied transporter neutral, transporter-transportee complex charged with ze of the transportee. Case II, transporter-transportee complex neutral, unoccupied transporter charged with $-ze$ of the transportee.

be discussed, the following nomenclature is used (see Fig. 1): state X_1 is the charged state inside as a particular portion, N_1, of the entire number, N, of the transporter and state X_2 is the charged state outside as another portion, N_2, of N. For this formalism, no a priori distinction is made as to whether the transporter is neutral and the transporter–transportee-complex is charged with ze (case I) or the transporter is charged with $-ze$ and the complex is neutral (case II). The following states (X_3, X_4, ... X_n) and the corresponding portions (N_3, N_4, ... N_n) of N in the cycle bear increasing indices up to n before the loop closes to state X_1 again. Referring to the order of the particular model (here two-, three-, and four-state models), the states X_i and their particular portions, N_i, will bear a prescript. For example, $^3N_2$ will be the portion of N of the charged state outside in the three-state model (see Fig. 1).

Class I models (Hansen et al., 1981) are discussed here in more detail, i.e., cyclic reaction schemes with one voltage-sensitive reaction step comprising two voltage-sensitive rate constants.

$$k_{12} = k_{12}^0 \cdot \exp\,[zeV/(2kT)] \tag{1a}$$

$$k_{21} = k_{21}^0 \cdot \exp\,[-zeV/(2kT)] \tag{1b}$$

where e, k, and T have their usual thermodynamic meaning, V is the transmembrane voltage, k_{12}^0 and k_{21}^0 are the two voltage-sensitive rate constants k_{12} and k_{21} at V = 0, and the factor ½ accounts for the assumption of a symmetric Eyring barrier. Since microscopic aspects are favored here, the molecular term "e/k" is used instead of the equivalent molar term "F/R," which may be more familiar.

The velocity of reactions that describe the association of substrate S depends on the particular substrate concentration. The corresponding (apparent) rate constants can be expressed as

$$k_s = k_s^0\,[S]^n \tag{2}$$

with k_s^0 describing the velocity of substrate association at 1 M substrate concentration and n being a stoichiometry coefficient. For changes in substrate concentration from [S] to [S]′ by a factor x, the apparent rate constants change from k to k′ = xk.

For ease of writing (and reading), we shall use symbols with just one character instead of employing many indices: for the two-state model, small greek letters; for the three-state model, capital latin letters; and for the four-state model small latin letters starting with α(A, a) for the charge transition from inside to outside, β(B, b) for the reverse reaction, γ(C, c) for the discharge outside, δ(D, d) for the reverse reaction, and so on following the reaction cycle. This nomenclature is illustrated in Fig. 1. For the two-state model only, the original denotation (Hansen et al., 1981) has been used more or less consistently by numerous authors. The conversion to the nomenclature used here is $\alpha = k_{io}$, $\beta = k_{oi}$, $\gamma = \kappa_{oi}$, and $\delta = \kappa_{io}$.

For the extension of the four-state model to a six-state model by an additional reaction loop for a second substrate, more rate constants are required (Figs. 3 and 6). If the second substrate is also charged (Fig. 3), the six-state model comprises two voltage-sensitive reaction steps. Thus, the current-voltage curves of this six-state model are not covered anymore by the class I model. For the reaction kinetic description of the additional loop, primed symbols are used in a symmetric arrangement to the unprimed parameters of the main loop.

Current–Voltage Curves

If the rate constants k_{ij} and their voltage-sensitivities (see Eqs. 1a and b) of an n-state model are known as well as the

density of transporter molecules, $N = \Sigma N_i$, the individual N_i can be calculated by solving a system of linear equations of the type

$$dN_i/dt = -N_i \cdot \sum_{j-1}^{n} k_{ij} + \sum_{j-1}^{n} (k_{ji}N_j) \qquad (3)$$

with $dN_i/dt = 0$ for steady-state conditions. With known N_i and k_{ij}, a comprehensive description of the steady-state properties of the model can be formulated. One of these properties is the current–voltage relationship. For a class I transporter, this steady-state current–voltage relationship is

$$I(V) = ze(N_1k_{12} - N_2k_{21}). \qquad (4)$$

Considering a transporter with a number of four or more distinct states, the explicit algebraic description of the system will become very large, even for class I transporters. In many cases, however, the algebra can be rewritten in a more compact form without any loss in accuracy. Such reductions can be used just for algebraic convenience or to subsume particular parts of the reaction system.

Principles of Model Reduction

Gross Rate Constants. The genuine information on the steady-state electrical properties of a class I model is given by its current–voltage curve, which is determined by four independent parameters (Hansen et al., 1981). In general, this is only sufficient to determine the four parameters for a two-state model. The question now is how such two-state parameters are related to the "true" model (in our case the four-state model). To treat this problem, we pick the reaction that is changed during the experimental procedure (here k_{12} and k_{21} due to V) and summarize the rest of the reaction cycle by introducing two gross rate constants for the forward and reverse reaction of the voltage-independent part of the reaction scheme. Gross rate constants can be written with a series of indices, marking the order of each state involved. The relationship between gross rate constants and individual rate constants is demonstrated by the following example where from the reaction chain

$$^3X_a \underset{^3k_{ba}}{\overset{^3k_{ab}}{\rightleftharpoons}} {}^3X_b \underset{^3k_{cb}}{\overset{^3k_{bc}}{\rightleftharpoons}} {}^3X_c \qquad (5)$$

the state ^3X_b is to be eliminated. A prescript (here 2 or 3) on the model parameters (N and k) indicates the number of states of the particular model under consideration.

To determine the gross rate constant $^3k_{abc}$ by which ^3X_a is converted to ^3X_c and the gross rate constant $^3k_{cba}$ for the reverse reaction, we start from the two differential equations

$$d^3N_a/dt = -{}^3k_{ab} \cdot {}^3N_a + {}^3k_{ba} \cdot {}^3N_b \qquad (6a)$$

$$d^3N_b/dt = {}^3k_{ab} \cdot {}^3N_a - ({}^3k_{ba} + {}^3k_{bc}) \cdot {}^3N_b + {}^3k_{cb} \cdot {}^3N_c. \qquad (6b)$$

For steady state conditions ($d^3N_b/dt = 0$), Eq. 6b can be solved for ^3N_b.

$$^3N_b = {}^3N_a \frac{^3k_{ab}}{^3k_{ba} + {}^3k_{bc}} + {}^3N_c \frac{^3k_{cb}}{^3k_{ba} + {}^3k_{bc}} \qquad (7)$$

and substituting this ^3N_b in Eq. 6a yields

$$d^3N_a/dt = -\frac{^3k_{ab} \cdot {}^3k_{bc}}{^3k_{ba} + {}^3k_{bc}} {}^3N_a + \frac{^3k_{cb} \cdot {}^3k_{ba}}{^3k_{ba} + {}^3k_{bc}} {}^3N_c \qquad (8a)$$

$$= -{}^3k_{abc} \cdot {}^3N_a + {}^3k_{cba} \cdot {}^3N_c \qquad (8b)$$

with the gross rate constants

$$^3k_{abc} = \frac{^3k_{ab} \cdot {}^3k_{bc}}{^3k_{ba} + {}^3k_{bc}} \qquad (9a)$$

$$^3k_{cba} = \frac{^3k_{cb} \cdot {}^3k_{ba}}{^3k_{ba} + {}^3k_{bc}} \qquad (9b)$$

Reserve Factors. The "reserve factors," r, as originally introduced by Hansen et al. (1981), have turned out to be somewhat inconvenient for practical use. Therefore, these reserve factors have been redefined by Mummert et al. (1981). In this study we use the reserve factors in the latter meaning and give a more explicit derivation so they can be used directly.

If an intermediate state (here ^3X_b) is formally omitted by introducing gross rate constants, care must be taken for the correct representation of the fluxes $J_i = N_ik_{ij}$. For the present example (reducing a three-state model to a two-state model), the law of mass conservation requires

$$N = {}^3N_a + {}^3N_b + {}^3N_c = {}^2N_a + {}^2N_c. \qquad (10a, b)$$

This means that the amount of ^3N_b to be omitted in the two-state formalism must be reflected by increased amounts of ^2N_a and ^2N_c compared with ^3N_a and ^3N_c

$$^2N_a = r_a {}^3N_a \qquad (11a)$$

$$^2N_c = r_c {}^3N_a \qquad (11b)$$

with the reserve factors r_a and r_c. These reserve factors can be obtained by Eq. 7, which shows that the intermediate ^3N_b can be expressed as a term of ^3N_a and another one of ^3N_c. Adding these expressions to the corresponding states yields

$$^2N_a = \left(1 + \frac{^3k_{ab}}{^3k_{ba} + {}^3k_{bc}}\right) {}^3N_a \qquad (12a)$$

$$^2N_c = \left(1 + \frac{^3k_{cb}}{^3k_{ba} + {}^3k_{bc}}\right) {}^3N_c \qquad (12b)$$

or by rearrangement and comparison with Eqs. 11a and b,

$$r_a = \frac{^3k_{ba} + {}^3k_{bc} + {}^3k_{ab}}{^3k_{ba} + {}^3k_{bc}} \qquad (13a)$$

$$r_c = \frac{^3k_{ba} + {}^3k_{bc} + {}^3k_{cb}}{^3k_{ba} + {}^3k_{bc}}. \qquad (13b)$$

To represent the true fluxes $^3N_ak_{abc}$ and $^3N_ck_{cba}$ correctly by the two-state formalism, the increased ^2N values must be balanced by decreased ^2k values;

$$^2k_{ac} = {}^3k_{abc}/r_a \tag{14a}$$

$$^2k_{ca} = {}^3k_{cba}/r_c. \tag{14b}$$

By repeated application of this procedure, parts of a reaction system can be summarized into one reaction step for steady-state conditions.

The Four-State Model and its Reductions

For a class I uniporter, we assume a real four-state model with one voltage-sensitive reaction describing the charge translocation between state $^4X_1$ and state $^4X_2$ (Fig. 1, *top*). Two cases must be distinguished: case I in which the transporter is neutral and the complex is charged and case II in which the transporter is charged and the complex is neutral. In these two cases, translocation steps and substrate reactions are immediately adjacent.

If intermediate reactions become relevant, the kinetic behavior of the system will again be different, which must be accounted for by one or more additional states in the reaction cycle. The kinetics of these cases are not explicitly discussed here (but see Hansen et al., 1981).

If in the four-state model (Fig. 1, *top*) the external substrate concentration is changed by a factor x′ for case I, the rate for substrate binding outside, d, becomes d′ = x′d, or, if the internal substrate concentration is changed by x″, g becomes g″ = x″g. For case II, the rates for substrate binding are c (outside) and h (inside) and will change to c′ = x′c or h″ = x″h, respectively (see Fig. 2).

Case I

Reduction of Four-State Model to Three-State Model. Upon a change in voltage and in external substrate, no rate constant of the part of the reaction scheme from state $^4X_3$ via state $^4X_4$ to state $^4X_1$ is affected (see Fig. 2, *left*) and the state $^4X_4$ can be eliminated. The reserve factor

$$r_3 = (e + f + g)/(f + g) \tag{15a}$$

must be considered for the rate constants (D and E), which start from the original state $^4X_3$, and

$$r_1 = (f + g + h)/(f + g) \tag{15b}$$

for A and F, which originate from the state $^4X_1$. This leads to three-state model parameters for control conditions (Eqs. 16a–21a in Table I) and for a change in external substrate concentration by x′ (compare Eqs. 16b–21b with Eqs. 16a–21a in Table I). Similarly, we eliminate state $^4X_3$ for an internal change in substrate concentration (″). For the entire procedure we must distinguish whether the three-state model is obtained by elimination of state $^4X_4$ (resulting three-state rate constants are marked with the index "o") or by elimination of state $^4X_3$ (resulting three-state rate constants are marked with the index "i", Eqs. 16c and d–21c and d in Table I).

Reduction to Two-State Model. For the further reduction to the two-state model, the indices i and o can be omitted because we now have a symmetric situation in which both $^4X_3$ and $^4X_4$ are eliminated. Applying the formalism of model reduction by elimination of the states $^4X_3$ and $^4X_4$ yields three sets of two-state parameters for the three experiments (control, change in external substrate concentration by x′, and change in internal substrate concentration by x″). For these three conditions, the two-state parameters as expressions of the four-state parameters (Eqs. 22–25) are listed in Table II.

Finally, the two-state parameters in terms of the three-state parameters (Eqs. 26–29) are listed in Table III for the three experimental conditions. These terms result from the elimination of the state $^3X_3$.

Each set of two-state parameters describes an individual current–voltage curve by the current–voltage equation of the two-state model (Eq. 30, Hansen et al., 1981), which is derived from the steady-state equations (see Eqs. 4 and 5) of the two-state model.

$$I(V) = ze\frac{\alpha\gamma - \beta\delta}{\alpha + \beta + \gamma + \delta} \tag{30}$$

with the voltage sensitivity in $\alpha = \alpha^0 \cdot \exp(zeV/(2kT))$ and $\beta = \beta^0 \cdot \exp(-zeV/(2kT))$ (compare Eqs. 1a and b). Four characteristic values, such as the equilibrium voltage (V_{i-o}), the short circuit current (I_{sc}) and saturation currents ($I_{s+} = \gamma ze$ and $I_{s-} = -\delta ze$), or the relative steepness (see below), must be determined from the measured current–voltage relationship and converted to the desired values of α, β, γ, and δ. This can be done algebraically using a set of four independent parameters or by fitting Eq. 30 to the data (Gradmann et al., 1982 *a*, *b*).

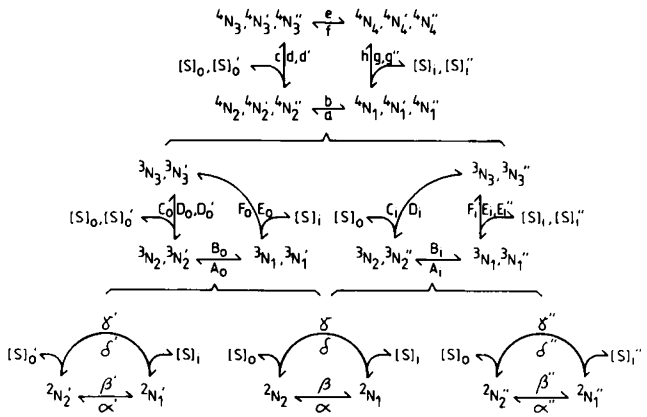

FIGURE 2 Nomenclature used for stepwise model reduction (*from top to bottom*) and for calculation (*from bottom to top*) of complete case I four-state model from three two-state models as obtained from three experiments (control, change in external (′) and in internal (″) substrate concentration) via two three-state models; for symbols see Fig. 1.

TABLE I
THREE-STATE PARAMETERS IN TERMS OF FOUR-STATE PARAMETERS

External substrate change (o), elimination of $^4N_4$		Internal substrate change (i), elimination of $^4N_3$		Eq. No.
Control	Change	Control	Change	
$A_o = a\frac{f+g}{f+g+h}$	$A'_o = A_o$	$A_i = a$	$A''_i = A_i$	(16a–d)
$B_o = b$	$B'_o = B_o$	$B_i = b\frac{d+e}{c+d+e}$	$B''_i = B_i$	(17a–d)
$C_o = c$	$C'_o = C_o$	$C_i = \frac{ce}{c+d+e}$	$C''_i = C_i$	(18a–d)
$D_o = d\frac{f+g}{e+f+g}$	$D'_o = x'd\frac{f+g}{e+f+g}$	$D_i = \frac{df}{d+e+f}$	$D''_i = D_i$	(19a–d)
$E_o = \frac{eg}{e+f+g}$	$E'_o = E_o$	$E_i = g\frac{d+e}{d+e+f}$	$E''_i = x''g\frac{d+e}{d+e+f}$	(20a–d)
$F_o = \frac{fh}{f+g+h}$	$F'_o = F_o$	$F_i = h$	$F''_i = h$	(21a–d)

Model reduction: cf. Figs. 1 and 2. Case I: transporter neutral, complex charged.

TABLE II
TWO-STATE PARAMETERS IN TERMS OF FOUR-STATE PARAMETERS

Control (a)	External substrate change (b)	Internal substrate change (c)	Eq. No.
$\alpha = a\frac{eg+dg+df}{eg+dg+df+he+hf+hd}$	$\alpha' = a\frac{x'd(f+g)+eg}{x'd(f+g+h)+eg+he+hf}$	$\alpha'' = a\frac{x''g(e+d)+df}{x''g(e+d)+df+he+hf+hd}$	(22)
$\beta = b\frac{eg+dg+df}{eg+dg+df+ce+cf+cg}$	$\beta' = b\frac{x'd(f+g)+eg}{x'd(f+g)+eg+ce+cf+cg}$	$\beta'' = b\frac{x''g(e+d)+df}{x''g(c+e+d)+ce+cf+df}$	(23)
$\gamma = \frac{ceg}{eg+dg+df+ce+cf+cg}$	$\gamma' = \frac{ceg}{x'd(f+g)+eg+ce+cf+cg}$	$\gamma'' = \frac{x''ceg}{x''g(c+e+d)+ce+cf+df}$	(24)
$\delta = \frac{hfd}{eg+dg+df+he+hf+hd}$	$\delta' = \frac{x'hfd}{x'd(f+g+h)+eg+he+hf}$	$\delta'' = \frac{hdf}{x''g(e+d)+df+he+hf+hd}$	(25)

Model reduction: cf. Figs. 1 and 2. Case I: transporter neutral, complex charged.

TABLE III
TWO-STATE PARAMETERS IN TERMS OF THREE-STATE PARAMETERS

Case I: transporter neutral, complex charged		Internal substrate change (c)	Case II: transporter charged, complex neutral	Eq. No.
Control (a)	External substrate change (b)		External substrate change (d)	
$\alpha = A\frac{D+E}{D+E+F}$	$\alpha' = A_o\frac{x'D_o+E_o}{x'D_o+E_o+F_o}$	$\alpha'' = A_i\frac{D_i+x''E_i}{D_i+x''E_i+F_i}$	$\alpha' = A_o\frac{D_o+E_o}{D_o+E_o+F_o} = \alpha$	(26)
$\beta = B\frac{D+E}{C+D+E}$	$\beta' = B_o\frac{x'D_o+E_o}{C_o+x'D_o+E_o}$	$\beta'' = B_i\frac{D_i+x''E_i}{C_i+D_i+x''E_i}$	$\beta' = B_o\frac{D_o+E_o}{x'C_o+D_o+E_o}$	(27)
$\gamma = \frac{CE}{C+D+E}$	$\gamma' = \frac{C_oE_o}{C_o+x'D_oE_o}$	$\gamma'' = \frac{C_ix''E_i}{C_i+D_i+x''E_i}$	$\gamma' = \frac{x'C_oE_o}{x'C_o+D_o+E_o}$	(28)
$\delta = \frac{DF}{D+E+F}$	$\delta' = \frac{x'D_oF_o}{x'D_o+E_o+F_o}$	$\delta'' = \frac{D_iF_i}{D_i+x''E_i+F_i}$	$\delta' = \frac{D_oF_o}{D_o+E_o+F_o} = \delta$	(29)

Model reduction: cf. Figs. 1 and 2; complete column *a* by subscripts "o" ("i") for comparison with columns b and d (c).

Relative Steepness. To examine class I current-voltage curves, four independent parameters are desired. Three of them, the saturation currents and the equilibrium voltage, can be read from the graphs. As a fourth parameter, the "relative steepness" has turned out to be useful. To define a measure for the general slope, a voltage difference, V_s, can be considered, which spans from a very positive voltage, V_1, to a very negative one, V_2, from the equilibrium where the currents differ from the respective saturation currents only by a very small fraction, p, of the entire current span, which is $ze(\delta + \gamma)$. Entering this condition into Eq. 30 yields

$$V_s = V_1 - V_2 = 2kT/(ze) \cdot \ln [\gamma\delta/(p^2\alpha\beta)]. \quad (31a, b)$$

To ensure $V_s > 0$, p must be chosen small enough. The expression of V_s means, roughly speaking, that for decreasing values of α and/or β the current-voltage curve is expanded over a wider voltage range. In turn, the ratio $\alpha\beta/(\gamma\delta)$ used below can be taken as a qualitative measure for the relative steepness. For large values of α^0 and β^0 compared with γ and δ, the actual slope of the current–voltage curve approaches a limiting value (Hansen et al., 1981) when neither α nor β vanish compared with γ and δ.

Thermodynamic Equilibrium. The employed models with different degrees of reduction from the "true" reaction scheme do equally account for the thermodynamic equilibrium by the following relationships:

$$q = aceg/(bdfh) = A_oC_oE_o/(B_oD_oF_o)$$
$$= A_iC_iE_i/(B_iD_iF_i) = \alpha\gamma/(\beta\delta). \quad (32a–d)$$

With the corresponding expressions q′ and q″ for the additional experimental conditions (′ and ″), the changes of the equilibrium potentials are

$$\Delta V' = [kT/(ze)] \cdot \ln (x') \quad (33a)$$

$$\Delta V'' = -[kT/(ze)] \cdot \ln (x'') \quad (33b)$$

with

$$x' = q/q' \quad (34a)$$

$$x'' = q''/q \quad (34b)$$

for the changes in external (x′) and internal (x″) substrate activities. From the relationships that can be derived from Eqs. 32 and 34, we shall explicitly use

$$x' = \alpha\beta'\gamma\delta'/(\alpha'\beta\gamma'\delta). \quad (35)$$

Algebraic Calculation of the Four-State Model

The goal is now to solve the inverse problem, i.e., to assemble the four-state model with eight rate constants from these three sets of two-state parameters. This can be done by the following stepwise procedure (see Fig. 2).

From Two Two-State Models to One Three-State Model. This extension will be given now explicitly for the comparison between the control experiment with experiment′ (at different external substrate concentration). From the two-state parameters one can form the auxiliary expression

$$M = \frac{\beta\gamma'}{\beta'\gamma} = \frac{D_o + E_o}{x'D_o + E_o} \quad (36a, b)$$

using Eqs. 27a and b and 28a and b, or by rearrangement of Eq. 36,

$$D_o = E_o \frac{M - 1}{1 - x'M}. \quad (37)$$

Furthermore, Eq. 29a and b can be solved for

$$F_o = \frac{\delta(D_o + E_o)}{D_o - \delta} = \frac{\delta'(x'D_o + E_o)}{x'D_o - \delta'} \quad (38a, b)$$

and rearranged to

$$D_o = \frac{E_o(x'\delta - \delta') + \delta'\delta(x' - 1)}{x'(\delta' - \delta)}. \quad (39)$$

Substitution of D_o from Eq. 37 in Eq. 39 yields after rearrangement

$$E_o = \frac{\delta'\delta(x' - 1)\{1 - x'[\beta\gamma'/(\beta'\gamma)]\}}{x'(\delta' - \delta)[\beta\gamma'/(\beta'\gamma) - 1] + (x'\delta - \delta')[\beta\gamma'(\beta'\gamma) - 1]} \quad (40)$$

in which the right hand term comprises only parameters that are known from the experiments.

The remaining five rate constants of the three-state model can now be calculated by backsubstitution: D_o by Eq. 39, F_o by Eq. 38a, C_o by Eq. 28a, B_o by Eq. 27a, and A_o by Eq. 26a.

Introducing Eq. 35 results in much simpler expressions for the three-state parameters in terms of 2-state parameters. A_o to F_o as functions of α to δ and α' to δ' are compiled in Table IV (Eq. $40A_o$–F_o) for a change in external substrate concentration.

The Second Three-State Model. To calculate the three-state parameters for a change in internal substrate concentration by x″, the analogue procedure can be used (not explicitly shown here) and yields another set of three-state parameters, A_i to F_i, as listed by Eq. $40A_i$–F_i in Table IV.

Merging Two Three-State Models into One Four-State Model. From the relationships between these two sets of three-state parameters and the underlying four-state model (Eqs. 20a–d to 25a–d), we can see that four of the eight four-state parameters are already known, namely a, b, c, and h. The goal now is to determine the remaining four rate constants (d, e, f, and g) from the

TABLE IV
THREE-STATE PARAMETERS IN TERMS OF TWO-STATE PARAMETERS

External substrate change (o)	Internal substrate change (i)	Eq. No.
$A_o = \frac{\alpha\alpha'(\beta'\gamma - \beta\gamma')}{\alpha\beta'\gamma - \alpha'\beta\gamma'}$	$A_i = \frac{\alpha(\beta\gamma'' - \beta''\gamma)}{\beta(\gamma'' + \delta) - \beta''(\gamma + \delta)}$	(40A)
$B_o = \frac{\beta(\alpha\delta' - \alpha'\delta)}{\alpha(\gamma + \delta') - \alpha'(\gamma + \delta)}$	$B_i = \frac{\beta\beta''(\alpha''\delta - \alpha\delta'')}{\alpha''\beta\delta - \alpha\beta''\delta''}$	(40B)
$C_o = Q_o \frac{\gamma(\alpha' - \alpha)}{\alpha(\gamma + \delta') - \alpha'(\gamma + \delta)}$	$C_i = Q_i \frac{\alpha''\delta(\beta'' - \beta)}{\alpha''\beta\delta - \alpha\beta''\delta''}$	(40C)
$D_o = \frac{\alpha'\delta(\beta'\gamma - \beta\gamma')}{\beta'\gamma(\alpha' - \alpha)}$	$D_i = \frac{\beta\gamma'' - \beta''\gamma}{\beta'' - \beta}$	(40D)
$E_o = \frac{\alpha\delta' - \alpha'\delta}{\alpha' - \alpha}$	$E_i = \frac{\beta''\gamma(\alpha''\delta - \alpha\delta'')}{\alpha''\delta(\beta'' - \beta)}$	(40E)
$F_o = Q_o \frac{\beta'\gamma(\alpha' - \alpha)}{\alpha\beta'\gamma - \alpha'\beta\gamma'}$	$F_i = Q_i \frac{\delta(\beta'' - \beta)}{\beta(\gamma'' + \delta) - \beta''(\gamma + \delta)}$	(40F)
with $Q_o = D_o + E_o$	and $Q_i = D_i + E_i$	

Model extension: cf. Figs. 1 and 2.

three-state parameters. This can be done, for example, in the following way: from Eq. 16a we obtain after rearrangement

$$M_1 = f + g = \frac{A_o F_i}{A_i - A_o} \quad \text{or} \quad g = M_1 - f. \qquad (41a\text{–}c)$$

Similarly from Eq. 17c

$$M_2 = d + e = \frac{B_i C_o}{B_o - B_i} \quad \text{or} \quad d = M_2 - e \qquad (42a\text{–}c)$$

M_1 and M_2 are auxiliary expressions only of known values. Substitution of f + g from Eq. 41a and d from Eq. 42c in Eq. 19a yields

$$e = \frac{M_1(M_2 - D_o)}{D_o + M_1}. \qquad (43)$$

Similarly, d + e from Eq. 42a and g from Eq. 41c in Eq. 20c yield

$$f = \frac{M_2(M_1 - E_i)}{E_i + M_2}. \qquad (44)$$

d and g can now be read from Eqs. 42c and 41c. The resulting four-state parameters in terms of the 3-state parameters are listed by Eqs. 45a–h in Table V. Only eight of the twelve three-state parameters appear in Eqs. 45a–h to express the eight four-state parameters because the two three-state models describe one and the same four-state model, which is totally determined by eight independent numbers.

Case II

Up to now, we have just treated case I (transporter neutral, complex charged), which permits the calculation of a higher-state model from current-voltage curves as measured at different substrate concentrations. For case II (see Fig. 1, *right*), the situation is not as favorable. In this case, it is c and h that are subjected to concentration dependent changes. Whereas the change in concentration on one side of the membrane caused all four two-state parameters to change in case I (compare Eqs. 22–25), these equations show for case II that, for instance, the change in external substrate concentration (c converts to x'c) will affect only β and γ but has no effect on α and δ. Since the positive saturation current is proportional to δ, it will stay constant.

This lack of effects on the two-state parameters already renders the reconstruction of the three-state model impossible. For these conditions, Eqs. 26a–29a convert to Eqs. 26d–29d as listed in Table III. Only two of the six three-state parameters can be determined. Eqs. 27a and d

TABLE V
FOUR-STATE PARAMETERS IN TERMS OF THREE-STATE PARAMETERS

Direct	Calculated	Eq. No.
$a = A_i$	$d = \frac{D_o[A_oF_i(B_o - B_i) + B_iC_o(A_i - A_o)]}{(B_o - B_i)(A_iD_o + A_oF_i - A_oD_o)}$	(45a,d)
$b = B_o$	$e = \frac{A_oF_i(B_iC_o + B_iD_o - B_oD_o)}{(B_o - B_i)(A_iD_o + A_oF_i - A_oD_o)}$	(45b,e)
$c = C_o$	$f = \frac{B_iC_o(A_oF_i + A_oE_i - A_iE_i)}{(A_i - A_o)(B_oE_i + B_iC_o - B_iE_i)}$	(45c,f)
$h = F_i$	$g = \frac{E_i[A_oF_i(B_o - B_i) + B_iC_o(A_i - A_o)]}{(A_i - A_o)(B_oE_i + B_iC_o - B_iE_i)}$	(45h,g)

Model extension, cf. Figs. 1 and 2.

yield (by elimination of C)

$$B_o = \frac{\beta'\beta(x' - 1)}{x'\beta' - \beta} \tag{46}$$

and Eq. 28a with d yield

$$E_o = \frac{\gamma'\gamma(x' - 1)}{x'\gamma - \gamma'}. \tag{47}$$

The remaining four parameters (A_o, C_o, D_o, and F_o) cannot be unambigously obtained because the available equations are not independent. With an arbitrary value for one of these values, the other three parameter values can be derived from Eqs. 16–21. Any set of such values for A, C, D, and F will yield the same two-state parameters in Eqs. 26a–29a and 26d–29d, and thus satisfy the experimental data. Therefore, case II obviously does not permit reconstructing a model with two more parameters from one additional current-voltage curve obtained by variation of the substrate concentration on one side of the membrane.

Extension of the Four-State Model to a Six-State Model

Current–Voltage Relationships. If the transport of two different substrates is mediated by the same transporter, a six-state model is required for the adequate reaction kinetic description. Such a six-state model is depicted in Fig. 3 for the particular situation when two substrates (K^+ and Na^+) compete for the same (uncharged) binding site. This model will be discussed in more detail because it will be used for the application below.

This six-state model can be reduced in terms of two two-state models that have separate pairs of lumped rate constants (α_1, β_1, and α_2, β_2) describing the two reaction chains for the two substrates (K^+ and Na^+ in our example) but the reorientation of the empty binding site (γ and δ) in common. The current–voltage relationship is

$$I(V) = ze\frac{(\alpha_1 + \alpha_2)\gamma - (\beta_1 + \beta_2)\delta}{\alpha_1 + \alpha_2 + \beta_1 + \beta_2 + \gamma + \delta} \tag{48}$$

in which the rate constants α_1, α_2, β_1, β_2, γ and δ are obtained by the above rules for model reduction.

$$\alpha_1 = acg/(Ar_4) \tag{49a$_1$}$$

$$\alpha_2 = a'c'g'/(A'r_4) \tag{49a$_2$}$$

$$\beta_1 = bdh/(Ar_3) \tag{49b$_1$}$$

$$\beta_2 = b'd'h'/(A'r_3) \tag{49b$_2$}$$

$$\gamma = e/r_3 \tag{49c}$$

$$\delta = f/r_4 \tag{49d}$$

with the reserve factors

$$r_3 = 1 + D/A + D'/A' \tag{50a}$$

$$r_4 = 1 + G/A + G'/A' \tag{50b}$$

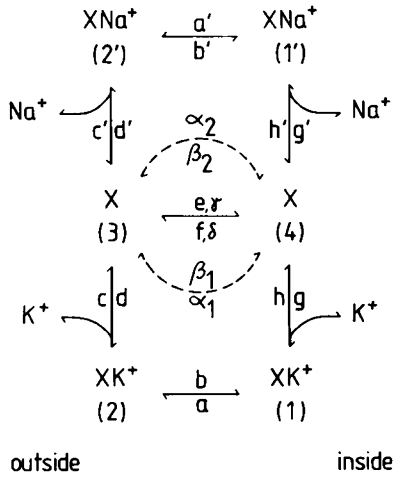

FIGURE 3 Extension of case I four-state model for uniport to six-state model for description of transport of competing substrates, here K^+ and Na^+: e, f = 0, ideal antiporter; d', g' = 0, four-state model for K^+ uniport; d, g = 0 (no data), Na^+ uniport; d, g' = 0, condition* ($[K^+]_o$, $[Na^+]_i = 0$); d', g = 0, condition** $[Na^+]_o$, $[K^+]_i = 0$.

and the auxiliary expressions

$$A = ac + bh + ch \tag{51a}$$

$$A' = a'c' + b'h' + c'h' \tag{51b}$$

$$D = d(a + b + d) \tag{51c}$$

$$D' = d'(a' + b' + d') \tag{51d}$$

$$G = g(a + b + c) \tag{51e}$$

$$G' = g'(a' + b' + c'). \tag{51f}$$

Note that the lumped rate constants (α_1, α_2, β_1 and β_2) as well as γ and δ now comprise voltage-sensitive and voltage-insensitive basic rate constants and the model is not of the class I type.

Rewriting Eq. 48 with respect to the voltage-dependent terms results in an expression of the form

$$I(V) = \frac{a_1U^2 + a_2U + a_3U^{-1} + a_5U^{-2}}{a_6U^2 + a_7U + a_8 + a_9U^{-1} + a_{10}U^{-2}} \tag{48a}$$

with $U = \exp[zeV/(2kT)]$ and coefficients a_i, which consist of terms of the fourteen rate constants of the six-state model at zero voltage. Compared with Eq. 30 for class I models, Eq. 48a demonstrates the more complicated current-voltage relationships of models with two voltage-sensitive reaction steps.

With respect to the application below, two experimental situations are of particular interest: condition* in which the main substrate (let's say K^+) is only inside and the alternate substrate' (let's say Na^+) is only outside, $[K^+]_i = [Na^+]_o > 0$, $[K^+]_o = [Na^+]_i = 0$ (d,g' = 0; α_2, $\beta_1 = 0$), and the corresponding condition** with $[K^+]_o = [Na^+]_i > 0$ and $[K^+]_i = [Na^+]_o = 0$ (d',g = 0; α_1, $\beta_2 = 0$). For these conditions the currents are in explicit terms of the basic

rate constants

$$I^* = ze\frac{acgeA' - b'd'h'fA}{(acgA' + fA)(A' + D') + (b'd'h' + eA)(A + G)} \quad (52)$$

$$I^{**} = ze\frac{a'c'g'eA - bdhfA'}{(a'c'g'A + fA)(A + D) + (bdh + eA')(A' + G')}. \quad (53)$$

For zero voltage, Eqs. 52 and 53 yield the short circuit currents I^*_{sc} and I^{**}_{sc}.

For very large voltage displacements these equations convert to the saturation currents

$$I^*_{s+} = ze\frac{ecgc'}{c(g + f)(c' + d') + ec'(g + c)} \quad (54)$$

$$I^*_{s-} = ze\frac{-fhd'h'}{h'(d' + e)(h + g) + fh(d' + h')} \quad (55)$$

$$I^{**}_{s+} = ze\frac{ecg'c'}{c'(g' + f)(c + d) + ec(g' + c')} \quad (56)$$

$$I^{**}_{s-} = ze\frac{-fhdh'}{h(d + e)(h' + g') + fh'(d + h)}. \quad (57)$$

Parameter Identification. To solve the inverse problem, Eqs. 54 to 57 can be used to calculate c', d', g', and h' when the unprimed rate constants are already known. For this purpose, Eqs. 54 and 57 can be solved for the ratios d'/c' and g'/h', respectively. By substitutions of d' and g' from these ratios in Eqs. 55 and 56, these equations can simultaneously be solved for the determination of the absolute values of c' and h'. Backsubstitution of c' and h' into Eqs. 54 and 57 yields d' and g'.

Finally, the short circuit currents I^*_{sc} and I^{**}_{sc} (see Eqs. 52 and 53) allow the determination of a'^0 and b'^0 since these equations can explicitly be rewritten in the form

$$I^*_{sc} = ze\frac{a'^\circ \cdot X_1 + b'^\circ \cdot X_2 + X_3}{a'^\circ \cdot X_4 + b'^\circ \cdot X_5 + X_6} \quad (58)$$

and

$$I^{**}_{sc} = ze\frac{a'^\circ \cdot Y_1 + b'^\circ \cdot Y_2 + Y_3}{a'^\circ \cdot Y_4 + b'^\circ \cdot Y_5 + Y_6} \quad (59)$$

where the X's and Y's are known. These Egs. 58 and 59 can simultaneously be solved for a'^0 and b'^0. The zero net current voltages

$$V^*(I = 0) = (-kT/(ze)) \cdot \ln(acgeA'/(b'd'h'fA)) \quad (60)$$

and

$$V^{**}(I = 0) = (-kT/(ze)) \cdot \ln(a'c'g'eA/(bdgfA')) \quad (61)$$

are not required to solve the inverse problem.

If the alternate substrate is absent, this six-state model is reduced to the case I four-state model (Fig. 2 *A, left*) because the two states in the alternate loop do not exist due to d', g' = 0.

APPLICATION

Example Data

During the past five years, nonlinear steady-state current-voltage relationships of several transporters under various experimental conditions have quantitatively been described by the two-state model (Hansen et al., 1981; Gradmann et al., 1982*a*; Beilby, 1984; Takeuchi et al., 1985) or even by a three-state model (Gradmann et al., 1982*b*; Fisahn et al., 1986) or a tentative four-state model (Slayman and Sanders, 1985). Current-voltage relationships from some plant membranes can be measured over a very wide voltage range (Gradmann, 1978; Beilby, 1987; Fisahn et al., 1986) of up to 500 mV. Fisahn et al. (1986) have demonstrated clear substrate-dependent saturation of the K^+ currents in *Nitella*, which are properly described by our model. However, serious problems with such macroscopic steady-state data include uncertainties as to whether (*a*) many slow transporters or few fast ones generate the macroscopic fluxes or (*b*) the nonlinearities arise in the active transporter itself or are due to voltage-dependent activation/inactivation of the individual transporters. These problems do not exist when patch-clamp data are available that were obtained from observations of individual transporter molecules. Therefore, we choose patch-clamp data for an example demonstration of the reaction kinetic analysis and interpretation of steady state current-voltage relationships.

Two patch-clamp studies are available to which the theory could be applied. For a K^+ channel in *Chara*, Lühring (1986) has presented a family of sigmoid current-voltage relationships. The saturation currents in these data are well determined. However, the experiments comprise only changes of the external K^+ concentration, which is only sufficient to determine the parameters of a three-state model.

The other source of suitable patch-clamp data (Schroeder et al., 1984, supplemented by some new data) describes an open K^+ channel in the plasmalemma of guard cells of *Vicia faba*. The (important) saturation currents in these experiments are not as well determined but are clearly indicated. On the other hand, these data are obtained from experimental conditions that make possible the determination of a six-state model. To demonstrate the capabilities (and difficulties) of the method, these data are treated in detail.

The original data from Schroeder et al. (1984) are replotted in Fig. 5. They consist of three sets of control experiments (sets of data I, II, and III measured at symmetrical 225 mM K^+ concentrations), two sets of experiment* (V and VI, external K^+ replaced by Na^+) and one set of experiment** (VII, internal K^+ replaced by Na^+). Additional data (set IV) from 225 mM K^+ inside

and 30 mM K^+ outside (experiment', without Na^+) are given in Fig. 4 together with the corresponding control experiment (set I) from the same patch.

Qualitative Inspection of Data

Symmetry. A rough inspection of Figs. 4 and 5 reveals that the current-voltage data appear to be distributed symmetrically about the origin. With the assumption of symmetry ($a^0 = b^0$, $c = h$, $d = g$, and $e = f$), some important features of the reaction system can be extracted from the I-V data points. For this purpose, the results from Fig. 4 are discussed first because they are expected to obey the simple four-state model for uniport.

Saturation. In the original communication (Schroeder et al., 1984), the central parts of the current-voltage data (sets I to III and V to VII; cf. Fig. 5) were approximated by ohmic conductances. However, for larger positive and negative voltage displacements, the measured currents display a clear tendency towards saturation. This observation also holds for the new data in Fig. 4. Observation of saturation currents means in terms of the general current–voltage equation of the two-state model (Eq. 30) that the voltage-insensitive parameters γ and δ in the denominator are not large compared to the voltage-sensitive ones (α and β). This is in contrast to the situation found in other channels such as gramicidin (Sandblom et al., 1977) in which the currents exponentially increase with larger voltage displacements in the investigated voltage

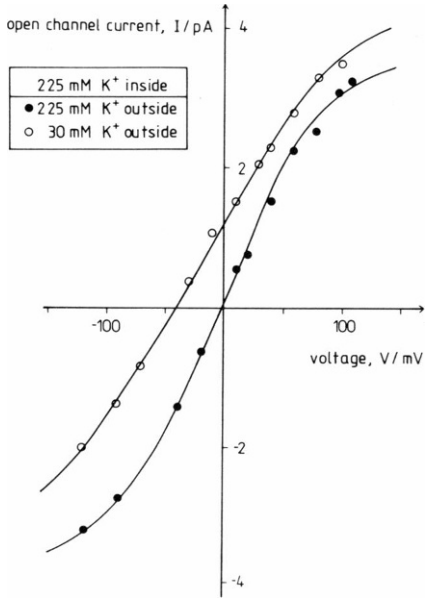

FIGURE 4 Current-voltage relationships of open K^+ channel in the plasma membrane of guard cell protoplasts from *Vicia faba*. *Filled circles*, same as in Fig. 5; *Open circles*, 225 mM K^+ inside, 30 mM K^+ outside, no Na^+; *Lines*, result of fitting these data to the unmodified case I three-state model (Figs. 1 B and 2, *middle left*) with its rate constants as listed in Table VII. Voltage V, inside with respect to outside; current I, positive outward current.

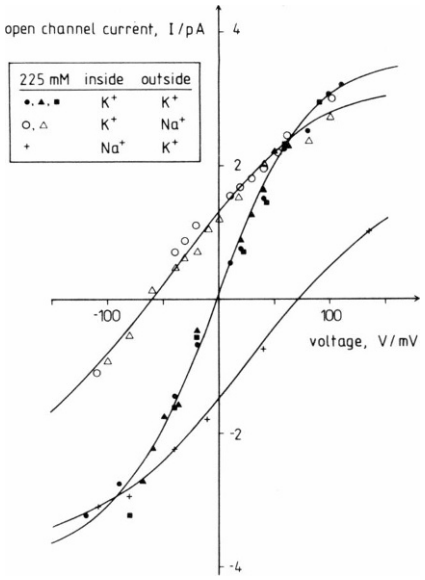

FIGURE 5 Current-voltage relationships of open K^+ channel in the plasma membrane of guard cell protoplasts from *Vicia faba*. Data points (SD of each point is between 0.2 and 0.3 pA) are replotted from Schroeder et al., 1984. Each symbol refers to a particular set of current-voltage data: *Closed symbols*, control conditions: 225 mM K^+ inside and outside; *Open symbols*, external K^+ replaced by Na^+; *Crosses*, internal K^+ replaced by Na^+; *Lines*, result of fitting these data to the case I six-state model (Fig. 3) with the 14 rate constants as listed in Table VIII. Voltage V, inside with respect to outside; current I, positive outward current.

range (in terms of Eq. 30, as long as $\gamma + \delta$ remains large compared to $\alpha + \beta$, the denominator will stay constant and the current–voltage characteristics will follow the exponential behavior of α or β in the numerator depending on the sign of the voltage).

The possibility that the observed saturations originate from limitation by diffusion can be ruled out by the following consideration. If the tendency toward saturation was due to limiting diffusion of the substrate to the binding site (a voltage-insensitive process in terms of the model), the approached saturation currents should be proportional to the substrate concentration in the charge delivering compartment. It can be seen from Eq. 25, for instance, that the equivalent of the negative saturation current, δ, will become proportional to the substrate binding rate, d, when d becomes very small. However, the data clearly disprove such a proportionality (compare negative currents of experiment' with control in Fig. 4 with respect to the apparent changes in substrate concentration x').

Case I or Case II?

Change of Saturation Currents. The data in Fig. 4 indicate an increase of the positive saturation current when the external substrate is reduced. Since case II of the four-state model predicts insensitivity of the positive saturation upon a change in external substrate concentration, case II must be rejected.

If in case I the expected changes in saturation currents were undetectably small, this would mean in terms of the four-state model that the dissociation rates c and h are much larger than all the other rate constants; for very large c and h values, Eq. 24a will convert to Eq. 24b [$\gamma = \gamma' = eg/(e + f + g)$] and Eq. 25a will convert to Eq. 25c [$\delta = \delta'' = df/(d + e + f)$].

Change in Relative Steepness. Since the relative steepness appears smaller in experiment' compared to the control experiment (the corresponding behavior can be expected for the missing symmetric experiment"), the expression $\alpha\beta/(\gamma\delta)$ must decrease for x' (and x") <1 in experiment' (and experiment"). This happens if e and f are small compared with d and g; with e, f $\ll$ d, g the expression $\alpha\beta/(\gamma\delta)$ as derived from Eqs. 22a to 25a converts to abdg/(chef). And with x' (and x") <1, replacement of d by x'd and g by x"g in the numerator will decrease the relative steepness. Corresponding changes of c and h for case II make the denominator (chef) smaller and, thereby, increase the relative steepness [abdg/(chef)].

Estimates of Some Model Parameters. Considering the changes of saturation currents ($I_{s+} = \gamma ze$ and $I_{s-} = \delta ze$), the voltage-independent parameters of the four-state model can be estimated without detailed computations. Since the saturation currents in Fig. 4 and 5 cannot immediately be read from the data, the fitted values of γ and δ (Table VI) are anticipated at this point for a numerical demonstration of the procedure.

From Eqs. 29a and b, (with subscript o) the relationship

$$D_o = (E_o + F_o)\frac{\delta' - x'\delta}{x'(\delta - \delta')} \tag{62}$$

can be obtained. With $\delta - \delta' \approx 0.1 \cdot \delta$ (Fig. 4, Table VI) and an apparent value for x' (= 0.225, cf. Table VII), which can be estimated from the change of the equilibrium voltage, Eq. 62 yields $D_o \approx 40(E_o + F_o)$. In other words, the small change in the negative saturation current means fast substrate association (large D_o) and slow translocation reactions (small E_o and F_o).

Furthermore, Eqs. 28a and b (with subscript o) yield for small E_o

$$C_o = D_o\frac{\gamma - x'\gamma'}{\gamma' - \gamma}. \tag{63}$$

Eq. 63 means that for small E_o the small change in the positive saturation current indicates a large ratio of C_o/D_o. With $\gamma' - \gamma \approx 0.1 \cdot \gamma$ (Table VI) and the same x' (0.225), Eq. 63 yields $C_o \approx 7.5 \cdot D_o$. Since the substrate association rate (D_o) includes the substrate concentration of 225 mM, the equilibrium constant for dissociation amounts to $C_o/(D_o/0.225\ M) \approx 1.7\ M-$.

For small E_o and F_o again, Eq. 29a yields an absolute value of $F_o \approx \delta \approx 2.6 \cdot 10^7\ s^{-1}$. Similarly, Eq. 28a yields (with known $C_o/D_o = 7.5$) after rearrangement an absolute value for $E_o = \gamma(1 + D_o/C_o) \approx 2.8 \cdot 10^7\ s^{-1}$. Inserting these values for E_o and F_o into Eq. 62 yields $D_o = 40(E_o + F_o) \approx 2.2 \cdot 10^9\ s^{-1}$ and $C_o = 7.5 \cdot D_o \approx 1.6 \cdot 10^{10}\ s^{-1}$.

Assuming symmetry and small values for e and f, the voltage-insensitive rate constants of the four-state model become $e = f = E_o = 2.8 \cdot 10^7\ s^{-1}$ (see Eq. 20a), $d = g = D_o = 2.2 \cdot 10^9\ s^{-1}$ (see Eq. 19a) and $c = h = C_o = 1.6 \cdot 10^{10}\ s^{-1}$.

The rate constants for substrate dissociation and association in the Na^+ loop of the six-state model can be estimated for the symmetrical situation as well. An approximate value for the ratio $c'/d' \approx 3$ can be determined by simplification of Eq. 54 for small values of e f and rearrangement to

$$c'/d' = I^*_{s+}/(eze - I^*_{s+}) \tag{64}$$

The ratio $c'/d' \approx 3$ refers again to a substrate concentration of 225 mM in these experiments. Thus, the dissociation constant for Na^+ amounts to $c'/(d'/0.225\ M) \approx 0.7\ M-$.

The ratio between the equilibrium constants for K^+ and for Na^+ (c/d vs. c'/d') is indicated by the saturation currents. Intersections such as in Fig. 5 occur if $cd'/(c'd) > 1$.

For an estimate of a'° and b'° the relative steepness can be used. The flattened shape of the current-voltage curves of experiment* and experiment** compared with the control current-voltage curve (Fig. 5) indicates that the relative steepness a'b'd'g'/(c'h'ef) of the Na^+ cycle is smaller than abdg/(chef) of the K^+ cycle. From this relationship, $a'(\approx b') < a(\approx b)$ can be concluded since the other parameters are already known.

To determine absolute values for the remaining rate constants, a more detailed analysis is required, which is described next.

Quantitative Analysis and Results

General Rules. The goal of the reaction kinetic analysis of the investigated channel is the determination of the fourteen rate constants of the six-state model (Fig. 3) from experimental current-voltage data. If sound data sets were available from control conditions, experiment' and experiment" for each of the two substrates, the two four-state models could be calculated (using Eqs. 40 and 45) separately and simply be merged to the six-state model by the common rate constants e and f.

In any case, the first task is to describe the individual sets of current-voltage data from different experimental conditions by the two-state model (individual fits of Eq. 30 to the particular data sets), which comprises the genuine information of class I reaction systems. Even if class I behavior cannot be assumed, such fits may frequently provide useful numbers for a preliminary characterization of the current–voltage relationships. Depending on the

significance of the data, the strategy of analysis must be adjusted to the particular situation. In general, such a strategy may comprise three steps, which are repeated at ascending levels.

The first step is to find start values for fitting a common model to data sets (current–voltage relationships) from different experimental conditions. This step can be done algebraically. However, the common model as obtained by such algebraic constructions may frequently be inconsistent, either directly (e.g., in the form of negative rate constants) or indirectly (e.g., if the two-state parameters as back-calculated from the common model deviate from the primary two-state parameters). Such inconsistencies may arise if the common model is either inappropriate or simply overdetermined by the empirical sets of two-state parameters. In the case of indirect inconsistency, the common model can be accepted if the back-calculated two-state parameters do not differ too much from the empirical ones. Direct inconsistencies can frequently be avoided by slight modifications of the empirical parameters.

The second step is the actual fitting of the parameters of the common model simultaneously to the original data from the different experimental conditions. Such multiparameter fits tend to converge at local error minima different from the "true" solution depending on the starting parameters. Therefore, the success of such fits pretty much depends on the proper choice of starting parameters in the first step.

The third step is an examination of the fit. The result can only be accepted if the entire set of original data from the different experiments are equally well described by the common model and by the individual two-state models.

Particular Example

Two-State Model. Sets of two-state parameters were fitted by Eq. 30 to each data set (I, II, III, and IV in Table VI) for which class I behavior is assumed. The results are listed in Table VI with the Gaussian standard deviation (SD) as a relative measure for the statistical quality. The results of two-state fits of experiment* (sets V and VI) and experiment** (set VII) are listed in Table VI as well for estimates of the saturation currents in these experiments (from γ and δ), although not Eq. 30 but Eqs. 52 and 53 apply for these experiments. These numbers may, therefore, only serve as phenomenological approaches.

Three-State Model. Beginning with the eight two-state parameters from the two data sets I and IV (Table VI), Eqs. $41A_o$–$41F_o$ yield consistent (positive) three-state parameters if, in contrast to the numbers listed in Table VI, the starting value of α'^0 is chosen smaller than α^0. With this precondition, simultaneous fitting of the three-state model to the two sets of data results in consistent three-state parameters as listed in Table VII. For a comparison, the intrinsic two-state parameters of this three-state model are listed in Table VII as well. Since the quality of this simultaneous fit (SD, $0.43 \cdot 10^6\ s^{-1}$) is essentially maintained compared with the individual two-state fits (mean of the two SD's, $0.38 \cdot 10^6\ s^{-1}$; see Table VI), the common three-state model seems to be adequate. A graphical representation of this fit is given by the smooth lines in Fig. 4. Calculating the equilibrium constant (Eq. 32b) for the control experiment from the fitted parameters results in q = 1.138, which can be taken to be in accord with microscopic reversibility which requires that q = 1.

TABLE VI
FITS OF THE SEVEN INDIVIDUAL SETS OF CURRENT-VOLTAGE DATA TO THE CLASS I TWO-STATE MODEL

	Control			Exp.'	Exp.*		Exp**
	I	II	III	IV	V	VI	VII
					Preliminary		
A Each set of data							
α^o	23.8	26.9	20.0	32.5	55.3	40.0	6.9
β^o	21.9	16.9	17.5	7.5	3.6	3.9	46.4
γ	26.3	29.4	32.5	27.5	17.5	17.5	8.8
δ	25.0	38.1	40.0	23.1	20.0	17.5	19.6
SD	0.43	0.94	0.64	0.33	1.16	0.75	0.93
B Each experiment							
α^0		30.0		32.5	34.4		6.9
β^0		27.5		7.5	3.8		46.4
γ		25.0		27.5	20.0		8.8
δ		25.6		23.1	16.9		19.6
SD		1.23		0.33	0.93		0.93

Rate constants α^0, β^0, γ^0, and δ^0, and Gaussian standard deviation (SD) expressed as $10^6\ s^{-1}$. Control: $[K^+]_i = [K^+]_o = 225$ mM. Experiment': $[K^+]_i = 225$ mM, $[K^+]_o = 30$ mM. Experiment*: $[Na^+]_o = [K^+]_i = 225$ mM Experiment**: $[Na^+]_i = [K^+]_o = 225$ mM. Preliminary: class II.

A slight systematic deviation may be seen in Fig. 4. Compared with the fitted curves, the data of the control experiment appear a little bit too flat and the data of experiment' a little bit too steep. These discrepancies are paralleled numerically by the small increase in SD and by the ratio α'^0/α^0, which is >1 (and inconsistent with the three-state model) before the fit (Table VI) and <1 (and consistent with the three-state model) after the fit (Table VII). Furthermore, the apparent x' = 0.225 is somewhat larger than the theoretical one (real change in external K^+ concentration, 30/225 = 0.133), which points to nonideal Nernstian behavior of the K^+ channel anyway, even if the given concentrations were corrected for the actual activities at the different ionic strengths used. No attempts were made to account for these observations.

Four-State Model. The corresponding experiment" (change of internal K^+ concentration in the absence of Na^+) is missing. However, the symmetrical current-voltage relationship of the control experiment suggests the reaction system for K^+ uniport to be approximately sym-

metrical. With this simplifying assumption of symmetry ($A_i = B_o$, $B_i = A_o$, $C_i = F_o$, $D_i = E_o$, $E_i = D_o$, and $F_i = C_o$), eight parameters of a (preliminary) symmetric four-state model were calculated (results not shown) by Eq. 45a–h. However, back-calculation of A_o to F_o from this four-state model by Eqs. 16a–21a, results in slightly different three-state parameters than listed in Table VII. These discrepancies may indicate some asymmetry in the "real" four-state model ($d \neq g$, $e \neq f$).

If data from experiment" were available, the six parameters of the second three-state model (A_i° to F_i) should be explicitly determined as well. The two sets of three-state parameters should then be used to calculated (by Eq. 45a–g) eight preliminary parameters of the (asymmetric) four-state model. These preliminary four-state parameters, in turn, provide (after adjustment for compatibility if necessary) the start parameters for finally fitting the eight parameters of the four-state model for K^+ uniport to the data of the three K^+ experiments (control, experiment', and experiment") in the absence of Na^+ as a competing substrate.

Six-State Model. Eqs. 54–59 can be used to calculate the six additional rate constants (a'^0, b'^0, c', d', g', and h') of the Na^+ loop with the information of the (preliminary) rate constants of the (symmetric) K^+ transport cycle plus the six characteristic currents from experiment* and experiment**: $I^*_{s+} = 3.2$ pA, $I^*_{s-} = -2.56$ pA, $I^{**}_{s+} = 2.11$ pA, and $I^{**}_{s-} = -3.63$ pA as estimated from preliminary two-state fits as listed in Table VI and $I^*_{sc} = 1.3$ pA, and $I^{**}_{sc} = -1.43$ pA as direct readings from Fig. 5. This direct calculation yields an inconsistent six-state model (i.e., negative values for a'^0 and b'^0) as a possible result of the unjustified assumption of symmetry in the K^+ cycle. Therefore, the three-state parameters, which were used to calculate the four-state model, have empirically been changed (by small amounts to $A_o = 32.9 \cdot 10^6\ s^{-1}$, $B_o = 167 \cdot 10^6\ s^{-1}$, $C_o = 10{,}220 \cdot 10^6\ s^{-1}$ and $D_o = 2{,}478 \cdot 10^6\ s^{-1}$; see Table VII; E_o and F_o are irrelevant for this calculation) to yield the start parameters (Table VIII) for fitting the six-state model to all seven sets of data from the four different experiments (control, experiment', experiment*, and experiment**).

TABLE VII
FIT OF SET I AND SET VII BY A COMMON THREE-STATE MODEL

Fitted three-state parameters		Resulting two-state parameters			
A_o°	32.6	α°	32.2	α'°	31.0
B_o°	166.9	β°	28.1	β'°	7.6
C_o	10,219.8	γ	24.1	γ'	26.1
D_o	2,043.8	δ	24.2	δ'	22.2
E_o	28.9	common SD: 0.43			
F_o	24.8				

Rate constants expressed as $10^6\ s^{-1}$; apparent x': $\alpha\beta'\gamma\delta'/(\alpha'\beta\gamma'\delta) = 0.225$

TABLE VIII
FIT OF THE FOURTEEN PARAMETERS OF THE SIX-STATE MODEL (FIG. 3) TO DATA OF FOUR EXPERIMENTS

Meaning	Parameter	Start	Fitted
K^+ translocation i → o	a°	167.0	148.8
K^+ translocation o → i	b°	167.0	204.5
K^+ debinding o	c	10,220.0	9,456.3
K^+ binding o	d	2,478.4	1,745.6
Empty site reorientation o → i	e	29.02	28.25
Empty site reorientation i → o	f	29.02	32.31
K^+ binding i	g	2,478.4	2,618.4
K^+ debinding i	h	10,220.0	8,278.8
Na^+ translocation i → o	a'°	3.58	6.44
Na^+ translocation o → i	b'°	2.40	9.97
Na^+ debinding o	c'	326.6	694.1
Na^+ binding o	d'	137.1	241.3
Na^+ binding i	g'	75.1	104.2
Na^+ debinding o	h'	301.4	321.7
SD		1.49	.88

Three data sets used for the control experiment ($[K^+]_i = [K^+]_o = 225$ mM). One data set used for experiment' ($[K^+]_i = 225$ mM, $[K^+]_o = 30$ mM). Two data sets used for experiment* ($[K^+]_i = 225$ mM, $[Na^+]_o = 225$ mM). One data set used for experiment** ($[Na^+]_i = 225$ mM, $[K^+]_o = 225$ mM). Rate constants at zero voltage expressed as $10^6\ s^{-1}$ and 225 mM substrate concentration. Start values and results of fit.

At this stage, the question arises as to whether the experimental information is sufficient to determine the 14 parameters of the six-state model. Since experiment" is missing, only six parameters (instead of eight) of the K^+ reaction cycle could be determined. However, from experiment* and experiment** not only the six characteristic currents are available but also the two zero-current voltages (Eqs. 60 and 61). This adds up to 14 parameters (six from control with experiment' plus eight from experiment* and experiment**), which are sufficient to determine the 14 rate constants of the six-state model without an excess degree of freedom.

The result of fitting the 14 rate constants of the six-state model to the seven sets of data (four different experiments) is listed in Table VIII. The fitted curves in Fig. 5 illustrate the successful description, which is confirmed by the common SD ($0.88 \cdot 10^6\ s^{-1}$) being almost identical with the mean SD ($0.86 \cdot 10^6\ s^{-1}$) from the four individual experiments (Table VIB). The equilibrium constant q = 1.9 (see Eq. 32a) in the Na^+ loop differs from the theoretical value of 1 for zero energy input. Considering the experimental data at hand, no particular attention was paid to this apparent discrepancy.

DISCUSSION

Four-State Model

From the various intrinsic properties of cyclic reaction systems, some characteristic features can be shown that become evident when considering the four-state model.

Saturation Currents. An important feature of cyclic models for ion transport is their capability to characterize the kinetics of the uncharged (loaded or unloaded) transporter, which results in the independence of the transport rates (saturation) on very large driving forces (i.e., far from thermodynamic equilibrium).

Electrical Charge of the Complex. For a cyclic reaction scheme of a uniporter, the question arises as to whether the loaded or the unloaded form of the transporter carries the charge. This difference is illustrated by cases I and II in Fig. 1. Two criteria that enable the distinction between these cases to be made are the dependence of the saturation currents and the relative steepness on the substrate concentration.

Effects of High Substrate Concentration. The observation that the conductance of ion channels decreases at very high substrate concentrations on both sides of the membrane has previously been explained by multiple binding sites (Sandblom et al., 1977). The cyclic model intrinsically accounts for this phenomenon; at high substrate concentrations on both sides (d and g being very large), the saturation currents will approach zero. This can be seen from Eqs. 24 and 25. The physical interpretation for this behavior is that inoccupancy of the empty states will interrupt the reaction cycle and no net current will occur. In this situation, however, the system will perform electroneutral substrate/substrate exchange and unidirectional (isotopic) fluxes will still take place.

Six-State Model

Intersections. Current–voltage curves of the four-state model for uniport cannot intersect because of a change in substrate concentration on one side of the membrane (Blatt, 1986). This can be seen by Eq. 28 in Table III for case I as well as for case II. The existence of intersections in the experimental data point to a more complicated reaction system. If a second (competing) substrate is present in the experiments, the four-state model for uniport must be extended to a six-state model by an extra reaction loop for the second substrate (Fig. 3). This six-state model does account for intersections under particular experimental conditions.

Symport. With slight modifications, the six-state model can also be used to describe a variety of transport phenomena, such as symport with ordered binding (Sanders et al., 1984) of charged and uncharged substrates.

For the description of symport of an electroneutral substrate S_2 with a charged substrate S_1, a modification (Fig. 6) of the six-state model of Fig. 3 can be used, where e, f = 0 and the binding steps for S_2 are h′ inside and c′ outside. Since only the reaction steps a and b are voltage-

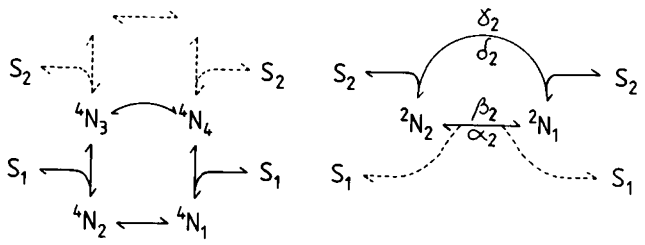

FIGURE 6 Example for further extension of model. *Left, bottom,* reaction scheme for transport of S_1 known; *top* (*dashed lines*), transport of S_2 to be determined. *Right,* reduction of known part to an alternate two-state model; reconstruction of the upper part by the analogue procedure as illustrated in Fig. 2.

sensitive, this system behaves as a class I model, i.e., its current–voltage relationships can be described by Eq. 30.

For the determination of the unprimed rate constants, the above four-state analysis provides the rate constants a, b, c, d, g, and h as well as α_2 and β_2 at given control concentrations of S_2 inside and outside. Subsequent reduction of the unprimed part of the system results in the pair α_1 and β_1. By the analysis of the changes of the current-voltage relationship upon internal and external concentration changes of S_2, the primed rate constants a′, b′, c′, d′, g′, and h′ can now be determined as well.

Ordered binding is assumed (Fig. 6) for this procedure. The more general problem of parameter identification of random binding models (Sanders, 1986, Läuger and Jauch, 1986) requires more rate constants and has not been treated yet. Another assumption for this description of symport is ideal coupling (i.e., e, f = 0). Nonideal coupling ("slipping") can be described by nonvanishing e and f (Sanders et al., 1984).

Antiport. The six-state model in Fig. 3 has been used to describe the kinetics of a K^+ channel that is also permeable for Na^+ but to a considerably smaller extent. The very model can also be viewed as the appropriate reaction scheme of a nonideal (slipping) antiporter for Na^+ and K^+. An ideal antiporter (e, f = 0) will provide strict coupling between the net fluxes of the two substrates. With identical charge in the two charge-carrying loops, there will be zero net current and the system will thus be electrically "silent."

Considering this striking similarity between the reaction kinetics of antiporters and channels, it is tempting to speculate that evolutionary similarities may exist as well. Since for the investigated system e and f turned out to be the smallest rate constants, it may be understood (from a reaction kinetic point of view) as an intermediate type of transporter between an ideal antiporter (e, f = 0) and an ideal electrophoretic channel (e, f ≫ other rate constants) without apparent saturation.

Similar considerations apply for symport. In this context, no fundamental difference seems to exist between various transport mechanisms. Gradual differences of the

same reaction scheme may enable the system to perform particular functions more or less specifically.

Alternate Models

A peculiar type of reaction kinetic models is treated here in detail. There are, of course, more elaborate models that account for some potentially important details, such as additional voltage-sensitivities, multiple binding sites, allosteric effects, intermediate states, and asymmetric Eyring barriers, which all may be anticipated for a very general model. However, the experimental information does not require incorporation of such details at the moment; it would prevent parameter identification due to excess degrees of freedom.

Nevertheless, some alternate models have also been tested. In particular, we have examined the more familiar approach of voltage-sensitive substrate reactions. For such a model, it is assumed that the reorientation of the loaded binding site occurs within a short distance in the membrane and the access rates of the ions from the bulk phases through a narrow ion conducting channel to the binding site plus its respective bindings are described by two voltage-dependent reactions (Mitchell, 1969; Woodhull, 1973; Maloney, 1982; Läuger, 1984; Dani, 1986; Restrepo and Kimmich, 1986). Voltage-sensitive binding has already been formulated in terms of our model as "Mitchellian behavior" by Hansen et al. (1981). In fact, with the simplifying assumption of the binding site being in the middle of the membrane, this alternate model does not require more parameters and may, therefore, appear as equivalent.

An intrinsic feature of this alternate model is the insensitivity of the saturation currents to the substrate concentration. But the data show that the two saturation currents (positive and negative) do depend on the substrate concentration. Therefore, this alternate model does not apply to the experimental data. Furthermore, application of this model to the data (Fig. 4) yields numerical values for the binding rate constants (at zero voltage) in the range of $10^9\ s^{-1}$, which appears unrealistically large with respect to the assumption of narrow channels. Moreover, the current–voltage relationship of this model with two voltage-sensitive reaction steps in series has also the form of Eq. 48a but with u being only $0.5 \cdot eV/(kT)$. These current–voltage relationships are smoother than those of the class I model, thus yielding worse fits even to an individual set of the presented current–voltage data.

The Method

The acquisition of rate constants for state-transitions in a (transporter) molecule has been regarded to be the domain of nonsteady-state analysis (Eigen, 1968; Läuger, 1973). However, based on theoretical grounds, curve-fitting of the steady-state data in Figs. 4 and 5 and Tables VI to VIII shows that the steady-state analysis allows the acquisition of such rate constants as well. In the analysis presented here, the determination of absolute rate constants from steady-state data becomes immediately possible through knowledge of the number of the involved transporter molecules, namely one, by studying individual transporters in patch-clamp experiments. The resolution of the steady-state analysis can be increased by studies of the effects of inhibitors and/or extended substrate actions when particular features (such as differences in saturation currents) become more evident. Even in these cases some of the determined rate constants may be gross rate constants including unknown reserve factors because of unidentified intermediate states. However, this problem is inherent to all kinds of kinetic analysis.

The determination of rate constants from steady-state analysis provides some advantages over the determination from nonsteady-state methods, namely the determination of rate constants of very fast reactions and the determination of rate constants with equal or hardly differing values. The first advantage results from the fact that very fast reactions may be beyond the temporal resolution of the recording apparatus. The second problem of the nonsteady-state approach results from the fact that exponential functions with similar time constants can hardly be distinguished. This problem does not exist for the presented steady-state analysis (compare data in Tables VI to VIII).

The disadvantage of the numerical steady-state analysis is the low sensitivity of the experimental parameters (i.e., the four two-state rate constants) on some of the model parameters (here the three-state and the four-state rate constants) thus making the determination of the rate constants very sensitive to the scatter in the experimental data.

RESULTS

Properties of the Channel

The numerical values for the six-state model in Table VIII show that the two K^+-transporter complexes are unstable. For K^+ the ratio of the rate constants for dissociation (c and h) to the apparent binding rates (d and g at a concentration of 225 mM) yielded 5.4 at the extraplasmatic and 3.2 at the intraplasmatic side of the membrane. In the K^+ loop, the voltage-sensitive reactions at $V = 0$ (a^0 and b^0) are considerably faster than the rate limiting reorientation of the unloaded binding site (e and f). This configuration resembles that of the transporter in Fig. 9 of Hansen et al. (1981) describing Mitchellian behavior, i.e., when no distinction is made as to whether the driving force (such as the proton motive force) for an ion results from the voltage or from the concentration gradient. In a class I model this equivalence of the driving forces can occur when the binding of the transportee (d and g in our model) is much slower than its dissociation from the complex (c and h in our model), and when the voltage-sensitive reactions (a and b in our model) are fast. In the extreme case of

Mitchellian behavior the substrate should affect the voltage-sensitive rate constants (α and β) of the two-state model exclusively. Table VI shows that the greater effect is on the voltage-sensitive rate constants (α and β). However, there is also an effect on the voltage-insensitive rate constants γ and δ, respectively). Thus, adopting the concept of a potassium driving force would not be appropriate for the data presented but can be anticipated for smaller substrate concentrations when the binding rates (d and g) become very small. Under these conditions, however, the saturation currents will appear unchanged and the determination of the four-state rate constants would be even more uncertain. On the other hand, the results suggest more accurate values for the four-state rate constants when greater substrate concentrations could be used.

In the Na^+ loop, the dissociation/association equilibria at 225 mM ($c'/d' = 2.9$ outside and $h'/g' = 3.1$ inside) are somewhat smaller than in the K^+ loop ($c/d = 5.4$ outside and $h/g = 3.2$ inside). The resulting ratios $cd'/(c'd)$, $hg'/(h'g) > 1$ reflect the intersections of the current-voltage curves in Fig. 5. This can be demonstrated for the positive saturation currents by comparing Eq. 24a with Eq. 54 or for the negative saturation currents by Eq. 25a and Eq. 57.

The K^+ selectivity of the channel is reflected by the absolute values of the rate constants, which are larger in the K^+ loop than in the Na^+ loop. However, this selectivity cannot be assigned to a specific reaction step since the relationships between the rate constants are similar in the K^+ loop and in the Na^+ loop.

Considering the ratios of the transmembrane reactions ($a^0/b^0 = 0.73$, $f/e = 1.15$, and $a'^0/b'^0 = 0.64$), the transporter seems to be asymmetric with a preference for the binding site oriented to the cytoplasmic compartment.

Physiological Function

Schroeder et al. (1984) have already demonstrated the possible role of K^+ channels in the function of guard cells in plants. One aspect may be added; plant cells do maintain Na^+ and K^+ gradients similar to those in animal cells. But there is no evidence for the operation of a Na^+/K^+ ATPase in plants. However, electrogenic H^+ ATPases are common in plant membranes, generating membrane voltages far beyond the equilibrium voltage of K^+. Thus, a K^+/Na^+ antiporter might mediate K^+ uptake and Na^+ extrusion. It has been demonstrated above that the investigated system does behave as a K^+/Na^+ antiporter, although not as an ideal one. The kinetic specification for this behavior consists of small values for e and f. In fact, this specification is also essential for saturation characteristics, which seem to be a common feature of the current-voltage relationships of open K^+ channels in plants (Schroeder et al., 1984; Lühring, 1986; Fisahn et al., 1986; Bertl and Gradmann, 1987). However, such a mechanism of voltage-driven K^+/Na^+ antiport could work only if the coupling were very tight (no slipping) and if the antiporter were electrophoretic, i.e., with a K^+/Na^+ stoichiometry >1. But this has not been shown here.

We thank Mr. Julian I. Schroeder for generously providing additional, unpublished data (in Fig. 4) and for critical reading of the manuscript.

This work was supported by the Deutsche Forschungsgemeinschaft.

Received for publication 12 March 1986 and in final form 24 September 1986

REFERENCES

Beilby, M. J. 1984. Current-voltage characteristics of the proton pump at *Chara* plasmalemma. I. pH dependence. *J. Membr. Biol.* 81:113–125.

Beilby, M. J. 1987. Electrophysiology of giant algal cells. *Methods Enzymol.* 4. In press.

Bertl, A., and D. Gradmann. 1987. Single-channel recordings from the plasmalemma of *Acetabularia*. *In* Plant Membrane Transport. N. A. Walker, editor. In press.

Blatt, M. R. 1986. Interpretation of steady-state current-voltage curves: consequences and implications of current subtraction in transport studies. *J. Membr. Biol.* 92:91–110.

Dani, J. A. 1986. Ion-channel entrances influence permeation. *Biophys. J.* 49:607–618.

Eigen, M. 1968. New looks and outlooks on physical enzymology. *Q. Rev. Biophys.* 1:3–33.

Fisahn, J., U.-P. Hansen, and D. Gradmann. 1986. Determination of charge, stoichiometry and reaction-constants from IV-curve studies on a K^+-transporter in *Nitella*. *J. Membr. Biol.* 94:245–252.

Gradmann, D. 1978. Green light (550 nm) inhibits electrogenic Cl^- pump in the *Acetabularia* membrane by permeability increase for the carrier ion. *J. Membr. Biol.* 44:1–24.

Gradmann, D., U.-P. Hansen, and C. L. Slayman. 1982*a*. Reaction-kinetic analysis of current-voltage relationships for electrogenic pumps in *Neurospora* and *Acetabularia*. *Curr. Top. Membr. Transp.* 16:257–276.

Gradmann, D., J. Tittor, and V. Goldfarb. 1982*b*. Electrogenic Cl^- pump in *Acetabularia*. *Philos. Trans. R. Soc. Lond. B. Biol. Sci.* 299:447–457.

Hansen, U.-P., D. Gradmann, D. Sanders, and C. L. Slayman. 1981. Interpretation of current-voltage relationships for "active" ion transport systems. I. Steady state reaction-kinetic analysis of Class-I mechanisms. *J. Membr. Biol.* 58:139–148.

Läuger, P. 1973. Carrier-mediated ion transport. *Science (Wash. DC).* 178:24–30.

Läuger, P. 1980. Kinetic properties of ion carriers and channels. *J. Membr. Biol.* 57:163–178.

Läuger, P. 1984. Thermodynamic and kinetic properties of electrogenic pumps. *Biochim. Biophys. Acta.* 779:307–341.

Läuger, P., and P. Jauch. 1986. Microscopic description of voltage effects on ion-driven cotransport systems. *J. Membr. Biol.* 91:275–284.

Lühring, H. 1986. Recording single K^+ channels in the membrane of cytoplasmic drop of *Chara australis*. *Protoplasma.* 133:19–28.

Maloney, P. C. 1982. Energy coupling to ATP synthesis by the proton-translocating ATPase. *J. Membr. Biol.* 58:43–55.

Mitchell, P. 1969. Chemiosmotic coupling and energy transduction. *Theor. Exp. Biophys.* 2:159–216.

Mummert, H., U.-P. Hansen, and D. Gradmann. 1981. Current-voltage curve of electrogenic Cl^- pump predicts voltage-dependent Cl^- efflux in *Acetabularia*. *J. Membr. Biol.* 62:139–148.

Restrepo, D., and G. A. Kimmich. 1986. The mechanistic nature of the membrane potential dependence of sodium-sugar cotransport in small intestine. *J. Membr. Biol.* 87:159–172.

Sandblom, J., G. Eisenman, and E. Neher. 1977. Ionic selectivity,

saturation and block in gramicidin A channels. I. Theory for the electrical properties of ion selective channels having two pairs of binding sites and multiple conductance states. *J. Membr. Biol.* 31:383–417.

Sanders, D., U.-P. Hansen, D. Gradmann, and C. L. Slayman. 1984. Generalized kinetic analysis of ion-driven cotransport systems: a unified interpretation of selective ionic effects on Michaelis parameters. *J. Membr. Biol.* 77:123–152.

Sanders, D. 1986. Generalized kinetic analysis of ion-driven cotransport systems. II. Random binding as a simple explanation for non-michaelian kinetics. *J. Membr. Biol.* 90:67–87.

Schroeder, J. I., R. Hedrich, and J. M. Fernandez. 1984. Potassium-selective single channels in guard cell protoplasts of *Vivia faba. Nature (Lond.).* 312:361–362.

Slayman, C. L., and D. Sanders. 1985. Steady-state kinetic analysis of an electroenzyme. *Biochem. Soc. Symp.* 50:11–29.

Takeuchi, Y., U. Kishimoto, T. Ohkawa, and N. Kami-ike. 1985. A kinetic analysis of the electrogenic pump of *Chara corallina.* II. Dependence of the pump on the external pH. *J. Membr. Biol.* 86:17–26.

Woodhall, A. 1973. Ionic blockage of sodium channels in nerve. *J. Gen. Physiol.* 61:687–708.